Original Article

Pantoprazole, a proton pump inhibitor, does not prevent botulinum toxin induced disuse osteopenia in mice

J.B. Vegger, A. Brüel*, J.S. Thomsen*

Department of Biomedicine, Aarhus University, Wilhelm Meyers Allé 3, DK-8000 Aarhus C, Denmark
* joint senior author

Abstract

Objectives: Pantoprazole is a proton pump inhibitor that has been shown to inhibit bone resorption. The aim of the study was to investigate whether pantoprazole can prevent development of botulinum toxin (BTX)-induced disuse osteopenia in mice. **Methods:** Forty-eight 16-week-old female C57BL/6J mice were randomized into 4 groups (n=12): Base, Ctrl, BTX, and BTX+Pan. The Base group was euthanized at study start. The BTX and BTX+Pan groups were immobilized by injections with BTX in one hind limb. The BTX+Pan group was injected i.p. daily with 100 mg pantoprazole per kg bodyweight. The mice were euthanized after 3 weeks of treatment. The skeletal status was investigated by DEXA, µCT, mechanical testing, dynamic bone histomorphometry, and RT-qPCR. The bone sites investigated were tibia, femur, L5 vertebra, and humerus. **Results:** Injections of BTX induced a pronounced and significant loss of bone density, microstructure, and strength in the immobilized hind limb. Furthermore, the localized intramuscular injections of BTX lead to a slight loss of bone and bone strength at the L5 vertebra and humerus. Treatment with pantoprazole did not have any bone protective or deleterious effects. **Conclusion:** Pantoprazole was unable to prevent the development of BTX induced disuse osteopenia in skeletally mature female C57BL/6J mice.

Keywords: Immobilization, PPI, MicroCT, Mechanical Testing, RT-qPCR

Introduction

Currently, most osteoporosis treatments aim at inhibiting osteoclasts thereby reducing bone resorption. Interestingly, this approach resembles the rare bone disease osteopetrosis that results from osteoclastic dysfunction, in which bone resorption is impaired creating a sclerotic and brittle skeleton[1]. Monogenetic mutations have been linked to this disease and in every second osteopetrotic patient a defect is found in the osteoclastic vacuolar H^+-ATPase proton pump

(V-ATPase)[2]. Consequently, acidification of the osteoclastic resorption pit is insufficient, which subsequently obstructs bone resorption and renewal of the skeleton[3]. Accordingly, by pharmaceutically blocking the V-ATPase in conditions characterized by high bone turnover, e.g. disuse osteopenia and osteoporosis, it might be possible to rescue or prevent the bone loss associated[4].

Proton pump inhibitors (PPIs) are widely used for treatment of stomach related acid disorders, e.g. reflux and ulcers. They work by irreversibly inhibiting the H^+/K^+-ATPase located in the canalicular membrane of parietal cells in gastric pits in the stomach, thereby reducing gastric acid production[5]. PPIs are pro-drugs, which are accumulated and activated in the acidic milieu that exists in the gastric crypts and in the osteoclastic resorption pits. *In vitro* studies have suggested that PPIs also have an inhibitory effect on the osteoclastic V-ATPase and thereby are able to reduce bone resorption[6-9]. On the contrary, *in vivo* studies have been less conclusive as they have shown either no or a slightly negative effect of PPI-treatment on bone integrity[10-13]. In rodents, pantoprazole, a PPI, has been revealed to delay fracture healing and calcium

phosphate cement resorption by decreasing both osteoclastic and osteoblastic activity[14,15].

Disuse osteopenia is characterized by a rapid bone loss caused by increased bone resorption and decreased bone formation[16,17]. As suggested, pantoprazole seems to inhibit or reduce osteoclastic activity, and may therefore be able to prevent disuse osteopenia. We and others have extensively investigated the botulinum toxin (BTX) model of disuse osteopenia, in which BTX is injected intramuscularly to paralyze one hind limb in rodents[18-22]. Paralyses is followed by a massive muscle atrophy and bone loss[17,20].

The aim of the present study was to prevent BTX induced disuse osteopenia by daily injections of pantoprazole in female C57BL/6J mice. The skeletal status was investigated with a series of different techniques including Dual Energy X-ray Absorptiometry (DEXA), micro Computed Tomography (µCT), mechanical testing, dynamical bone histomorphometry, and Reverse Transcription quantitative Polymerase Chain Reaction (RT-qPCR).

Materials and methods

Animals

Forty-eight 16-week-old female C57BL/6J mice (Taconic), with a mean body weight (BW) of 22.3±0.8 g, were housed at 20°C with a 12/12 h light/dark cycle. The animals had free access to tap water and standard mice chow (1324, Altromin).

At the age of 15 weeks, one week prior to study start, the animals were randomized according to their BW into 4 groups (n=12): Base, Ctrl, BTX, and BTX+Pan. At study start, the mice in the BTX groups were injected i.m. with 20 IU BTX (Botox, Allergan) per kg BW, distributed equally into the quadriceps muscle and calf muscles of the right hind limb. The Ctrl group was injected i.m. with saline in the same regimen as the BTX injections. The BTX+Pan group was injected i.p. with 100 mg pantoprazole (Pantoloc, Takada Pharma) per kg BW daily. The dosage was chosen based on the study by Histing et al., showing that pantoprazole inhibits fracture healing in mice[14]. The Ctrl and BTX groups were injected i.p. with saline. The mice were injected i.p. with alizarin (20 mg/kg), calcein (20 mg/kg), and tetracycline (20 mg/kg) 12, 8, and 4 days before euthanasia, respectively.

The treatment lasted three weeks after which the mice were euthanized by an overdose of anesthesia (IsoFlo Vet, Orion Pharma Animal Health) and removal of the heart. Each mouse received the last i.p. injection 6 h prior to euthanasia. One mouse in the BTX+Pan group was euthanized prematurely due to an ileus-like condition. The Base group was euthanized at study start to serve as baseline.

At euthanasia, the right tibiae were quickly isolated and carefully cleaned from soft tissue. The distal part was snap frozen in liquid nitrogen and stored at -80°C, while the proximal part was immersion-fixed in 0.1 M sodium phosphate buffered formaldehyde (4% formaldehyde, pH 7.0) for 48 h and then stored in 70% ethanol. The rectus femoris muscles were isolated and the wet weight determined. The right femora, right humeri, and L5 vertebrae were isolated, carefully cleaned from soft tissue, and stored in Ringer's solution at -20°C. The length of the femora and humeri were measured with a digital sliding caliper.

Dual energy X-ray absorptiometry (DEXA)

The femora and humeri were placed in a DEXA scanner (Sabre XL, Norland Stratec) and scanned with an isotropic pixel size of 0.1 mm. Bone mineral content (BMC) and areal bone mineral density (aBMD) were determined for the whole femur and humerus. Quality assurance was performed by scans of the two solid-state phantoms provided with the scanner.

Micro computed tomography (µCT)

The femoral mid-diaphysis, distal femur, L5 vertebra, humeral mid-diaphysis, and proximal humerus were scanned in a desktop µCT scanner (Scanco µCT 35, Scanco Medical AG). The femoral and humeral mid-diaphyses were scanned with an isotropic voxel size of 7 µm, X-ray voltage of 55 kVp and current of 145 µA, and an integration time of 300 ms. The distal femur and proximal humerus were scanned with an isotropic voxel size of 3.5 µm, X-ray voltage of 55 kVp and current of 145 µA, and an integration time of 800 ms. The L5 vertebra was scanned with an isotropic voxel size of 6 µm, X-ray voltage of 70 kVp and current of 114 µA, and an integration time of 800 ms. Volumes of interest (VOI) were analyzed with the software provided with µCT scanner (version 6.5). The threshold used for segmentation of the 3D data was automatically determined as the minimum point between the marrow and the bone peak in the attenuation histogram using IPL (version 5.11).

The femoral diaphysis was analyzed by placing an 819-µm-high VOI in the middle of the scanned region (Figure 1). The 3D data sets were low-pass filtered using a Gaussian filter (σ=0.8, support=1) and segmented with a fixed threshold filter (556.4 mg HA/cm^3). The humeral diaphysis was analyzed by placing a 420-µm-high VOI including cortical bone only between the deltoid tuberosity and epicondyles (Figure 1). The 3D data sets were low-pass filtered using a Gaussian filter (σ=0.8, support=1) and segmented with a fixed threshold filter (550.2 mg HA/cm^3). The cortical bone analysis included: Bone area, tissue area, marrow area, polar moment of inertia, and bone material density.

The distal femoral metaphysis was analyzed by placing a 1-mm-high VOI 0.2 mm proximal to the growth plate including trabecular bone only (Figure 1). The 3D data sets were low-pass filtered using a Gaussian filter (σ=1, support=2) and segmented with a fixed threshold filter (517.3 mg HA/cm^3). The distal femoral epiphysis was analyzed by placing a VOI distal to the growth plate until the intercondylar fossa including trabecular bone only (Figure 1). The 3D data sets were low-pass filtered using a Gaussian filter (σ=1, support=2) and segmented with a fixed threshold filter (525.5 mg HA/cm^3).

The L5 vertebral body was analyzed by placing a VOI between the primary spongiosa including trabecular bone
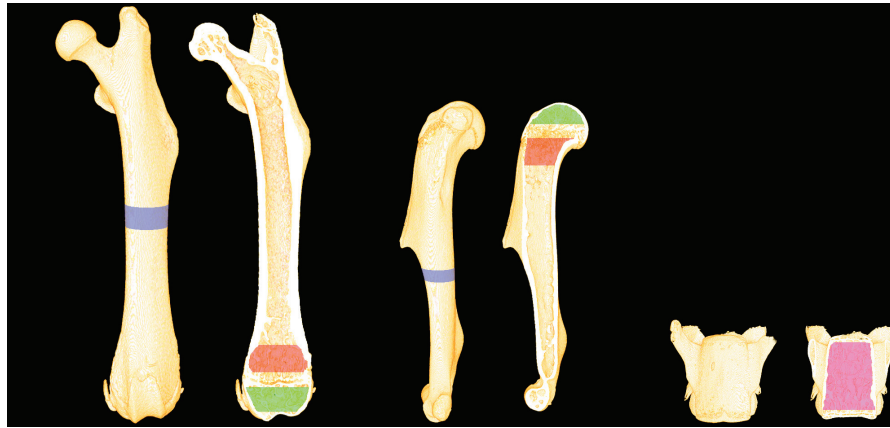
Figure 1. Volumes of interest (VOI) analyzed by µCT. The size of the femur, humerus, and vertebra are proportional to each other. The blue area represents the VOI at the diaphyses, the red area represents the VOI at the metaphyses, the green area represents the VOI at the epiphyses, and the pink area represents the VOI at the corpus vertebra.

only (Figure 1). The 3D data sets were low-pass filtered using a Gaussian filter (σ=1.3, support=2) and segmented with a fixed threshold filter (531.7 mg HA/cm^3).

The proximal humeral metaphysis was analyzed by placing a 1-mm-high VOI 0.2 mm distal to the growth plate including trabecular bone (Figure 1). The 3D data sets were low-pass filtered using a Gaussian filter (σ=1.3, support=2) and segmented with a fixed threshold filter (525.5 mg HA/cm^3). The proximal humeral epiphysis was analyzed by placing a VOI in the humeral head including the trabecular bone only (Figure 1). The 3D data sets were low-pass filtered using a Gaussian filter (σ=1.3, support=2) and segmented with a fixed threshold filter (535.8 mg HA/cm^3). The trabecular bone analysis included: trabecular bone volume fraction (BV/TV), trabecular thickness (Tb.Th), trabecular number (Tb.N), trabecular separation (Tb.Sp), connectivity density (CD), structure model index (SMI), and bone material density.

The µCT analyzes were performed according to the current guidelines[23]. Quality assurance was performed by weekly (density) and monthly (geometry) scans of the solid-state calibration phantom provided with the scanner. 3D visualization and imaging was performed using Amira (version 5.6.0, FEI).

Mechanical testing

The fracture strength of the femoral and humeral diaphysis was determined with a three point bending test. After the µCT scans, the femora and humeri were placed on a custom-made testing jig, supporting the proximal and distal part of the shaft. The distance between the two supporting rods was 7.1 mm. Load was applied at the midpoint of the femora and humeri in an anterior-posterior direction at a constant deflection rate of 2 mm/min until fracture using a materials testing

machine (5566, Instron). Subsequently, the proximal part of the femora was placed in another custom made fixation jig for femoral neck testing supporting the shaft under the neck. Load was applied to the top of the femoral head with a constant deflection rate of 2 mm/min until fracture of the femoral neck.

After the µCT scans, the L5 vertebrae were prepared for mechanical testing. The vertebral bodies were isolated by carefully removing the posterior arch and the cranial and caudal intervertebral discs. The height of the vertebral body was measured with a digital micrometer screw gauge and then placed in the materials testing machine. Load was applied in a cranial-caudal direction with a constant deflection rate of 2 mm/min until fracture.

Dynamic bone histomorphometry

After mechanical testing, the distal part of the femora were immersion-fixed in 0.1 M sodium phosphate buffered formaldehyde (4% formaldehyde, pH 7.0) for 48 h, dehydrated in ethanol, embedded undecalcified in methylmetacrylate, and 7-µm-thick sections were cut using a hard tissue microtome (RM 2065, Leica). The sections were mounted unstained on microscope slides and placed in a microscope (Eclipse 80i, Nikon) equipped for fluorescence microscopy. The stereology system newCAST (Version 6.4.1.2240, Visiopharm) was then used to count intersections with fluorochrome labels. Briefly, a region of interest (ROI), excluding cortical bone, was placed at the distal femoral epiphysis. In addition, a 1000-µm-high ROI, excluding cortical bone and primary spongiosa, was placed 200 µm proximal to growth plate covering the distal femoral metaphysis. At a magnification of ×200, a line grid was superimposed onto fields of view that covered 100% of the ROIs. The line grid was used to count

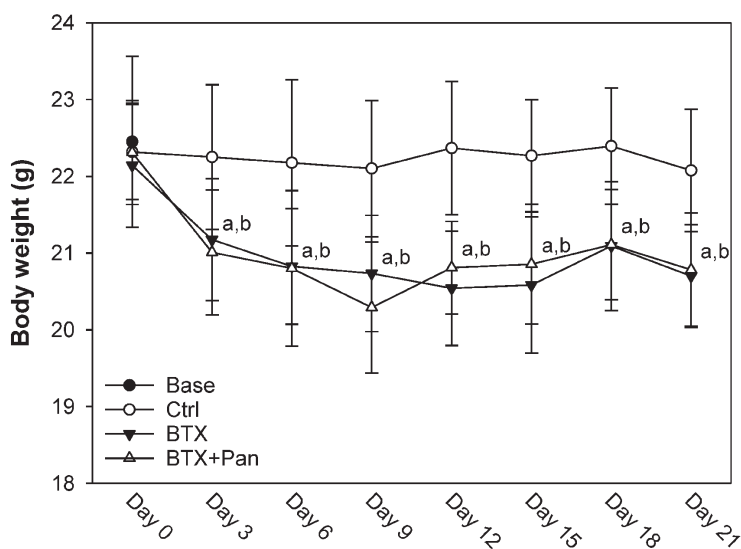**Figure 2.** Temporal development in body weight. [a] denotes a significant difference from Base and [b] donates a significant difference from Ctrl. Mean±SD.

Table 1. Weight of the rectus femoris muscles, length of the femora and humeri, and height of the corpus of the L5 vertebrae.

	Rectus femoris muscle mass (mg)	Femur length (mm)	L5 corpus height (mm)	Humerus length (mm)
Base	67.5 ± 5.2	15.32 ± 0.32	2.67 ± 0.16	11.80 ± 0.13
Ctrl	61.8 ± 6.5 [a]	15.48 ± 0.15	2.81 ± 0.14	11.90 ± 0.09
BTX	33.9 ± 5.1 [a,b]	15.37 ± 0.38	2.75 ± 0.13	11.84 ± 0.14
BTX+Pan	31.9 ± 4.7 [a,b]	15.54 ± 0.26	2.75 ± 0.11	11.87 ± 0.14
[a] denotes a significant difference from Base and [b] denotes a significant difference from Ctrl. Mean ± SD.				

intersections between the fluorochrome labels, while the distance between two fluorochrome labels was determined using the ruler tool in newCAST. Mineralizing surfaces (MS/BS), mineral apposition rate (MAR), and bone formation rate (BFR/BS) were determined.

The proximal part of the tibiae were decalcified using formic acid, dehydrated, embedded in paraffin, and cut into 2-µm-thick sections using a microtome (RM 2165, Leica). The sections was immunohistochemically stained for cathepsin K (APO8851PU-N, Acris) as described earlier[24]. The sections were scanned in a digital slide scanner (NanoZoomer-XR, Hamamatsu) and analyzed using newCAST. A 1000-µm-high ROI, excluding cortical bone and primary spongiosa, was placed 200 µm distal to the growth plate. At a magnification of ×600, a line grid was superimposed onto fields of view that covered 100% of the ROI. The line grid was used to count intersections with osteoclasts and bone surfaces, and the percentage of osteoclast covered bone surfaces (Oc.S/BS) was calculated.

Table 2. DEXA of the whole femur and humerus.

|	BMC (mg)	aBMD (mg/cm²)
Femur		
Base	15.0 ± 1.2	44.3 ± 1.7
Ctrl	16.3 ± 0.9 [a]	47.3 ± 1.5 [a]
BTX	11.3 ± 0.7 [a,b]	35.7 ± 1.4 [a,b]
BTX+Pan	11.3 ± 0.7 [a,b]	35.1 ± 1.4 [a,b]
Humerus		
Base	8.6 ± 1.1	43.1 ± 3.1
Ctrl	8.6 ± 1.2	40.8 ± 3.3
BTX	8.5 ± 1.1	42.0 ± 3.1
BTX+Pan	7.8 ± 1.1	37.9 ± 2.5 [a,b,c]
Bone mineral content (BMC). Areal bone mineral density (aBMD). [a] denotes a significant difference from Base, [b] denotes a significant difference from Ctrl, and [c] denotes a significant difference from BTX. Mean ± SD.		
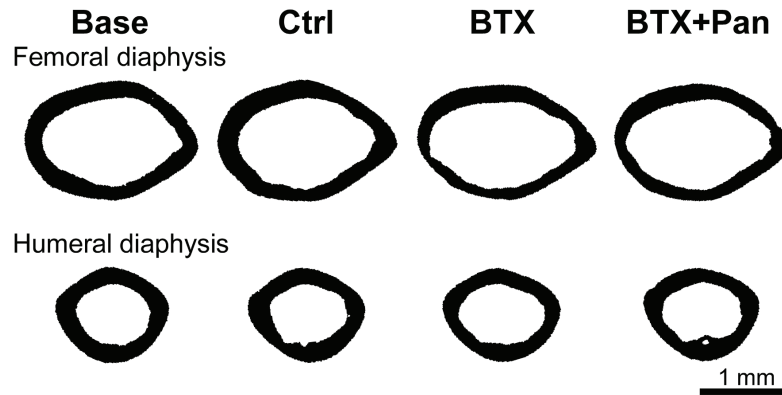
Figure 3. Transverse sections of the femoral and humeral mid-diaphysis acquired from the µCT scans. The samples shown are those closest to the mean values of the respective groups.

Table 3. µCT of the femoral and humeral mid-diaphyses.

	Bone area (mm²)	Marrow area (mm²)	Tissue area (mm²)	Polar moment of inertia (mm²)	Bone material density (mg/cm²)
Femoral mid-diaphysis					
Base	0.74 ± 0.03	1.02 ± 0.05	1.76 ± 0.08	0.35 ± 0.03	1126 ± 10
Ctrl	0.78 ± 0.04 [a]	1.00 ± 0.07	1.78 ± 0.11	0.37 ± 0.04	1141 ± 5 [a]
BTX	0.64 ± 0.03 [a,b]	1.07 ± 0.06 b	1.72 ± 0.05	0.30 ± 0.02 [a,b]	1130 ± 9 [b]
BTX+Pan	0.64 ± 0.04 [a,b]	1.07 ± 0.06 b	1.71 ± 0.08	0.30 ± 0.03 [a,b]	1130 ± 7 [b]
Humeral mid-diaphysis					
Base	0.50 ± 0.02	0.41 ± 0.02	0.91 ± 0.04	0.10 ± 0.01	1141 ± 14
Ctrl	0.51 ± 0.02	0.42 ± 0.02	0.93 ± 0.04	0.11 ± 0.01	1152 ± 10
BTX	0.49 ± 0.03	0.44 ± 0.02 [a,b]	0.93 ± 0.04	0.11 ± 0.01	1150 ± 10
BTX+Pan	0.48 ± 0.02	0.44 ± 0.01 [a,b]	0.93 ± 0.02	0.10 ± 0.01	1152 ± 11
[a] *denotes a significant difference from Base and* [b] *denotes a significant difference from Ctrl. Mean ± SD.*					

Reverse transcription quantitative polymerase chain reaction (RT-qPCR)

Six distal tibiae from each group were used for RT-qPCR. The distal tibiae were grinded in 1.5 ml microtubes with a micropestle (VWR), while kept frozen on dry ice in a special metal alloy microtube-rack (CoolRack M30 PF, BioCision) to minimize RNase activity. Lysis buffer from a PureLink RNA Mini kit (Ambion) was added and the pulverized bone was homogenized with rotor/stator homogenizer (VDI 12, VWR). RNA was isolated and purified with the PureLink RNA Mini kit. RNA quality was checked by running 1 µg total RNA on an agarose gel. 1 µg total RNA was transcribed into cDNA using qScript cDNA SuperMix (Quanta Biosciences). cDNA was diluted 1:5 with DEPC-treated water and 2 µl diluted cDNA was used in each reaction. PerfeCTa qPCR FastMix II (Quanta Biosciences) and TaqMan Gene Expression Assays (LifeTechnologies) was used with the following amplification protocol; hot start 95°C for 30 s followed by 40 cycles of amplification and quantification at 95°C for 3 s and 60°C for 30 s on a LightCycler 480 (Version 1.5, Roche). The studied genes were *Bglap* (osteocalcin) (Mm03413826_mH), *Ctsk* (cathepsin K) (Mm00484039_m1), *Nfatc1* (nuclear factor of activated T-cells, cytoplasmic 1) (Mm00479445_m1), *Rankl* (receptor activator of nuclear κ-B ligand) (Mm00441906_m1), *Opg* (osteoprotegerin) (Mm01205928_m1), and *Atp6v0d2* (V-type proton ATPase subunit d2) (Mm01222963_m1). Each sample was run in triplicates, and normalized to the reference genes *B2m* (beta-2 microglobulin) (Mm00437762_m1) and *Gapdh* (glyceraldehyde-3-phosphate dehydrogenase) (Mm99999915_g1).

Statistics

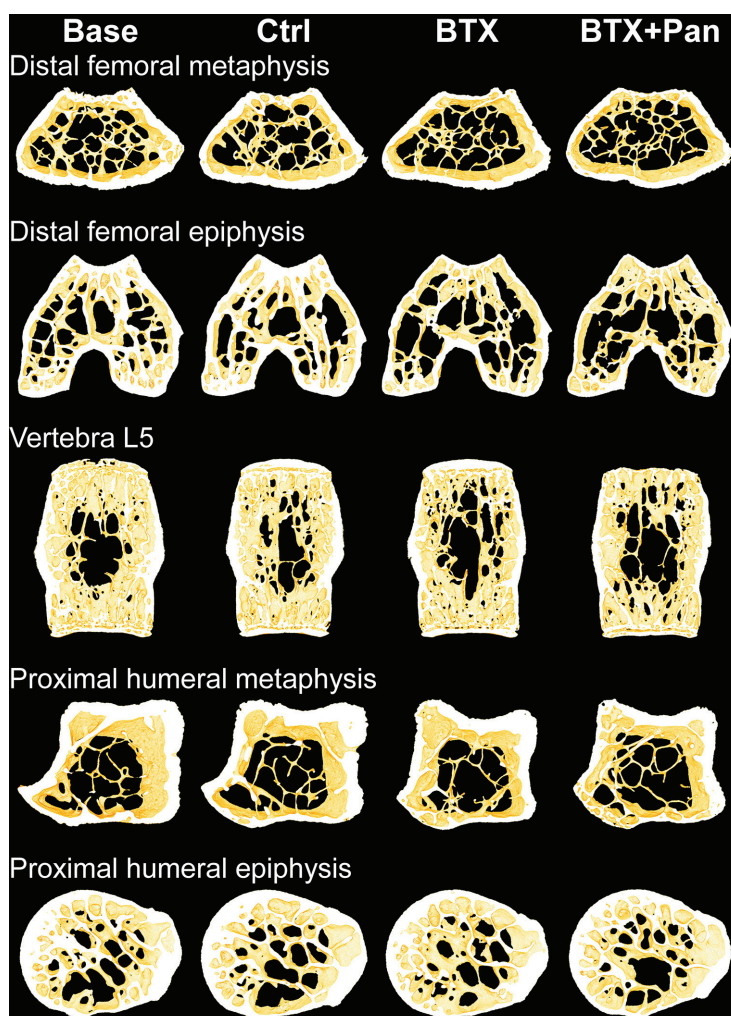Data are given as mean ± SD. Differences between the groups were analyzed by a parametric one way ANOVA,

Figure 4. 3D images reconstructed from the μCT scans. The size of the different bone sites are not proportional to each other. The samples shown are those closest to the mean values of the respective groups.

whenever normal distribution requirements were met or otherwise by a non-parametric Kruskal-Wallis test. When significant variance was found, multiple comparisons between the groups were performed with the Student-Newman-Keuls test. Results were defined as statistically significant, if the two-tailed $p<0.05$. The statistical analyzes and graph drawing was performed using SigmaPlot (Version 13.0, Systat Software).

Results

Animals

The BTX-injected mice rapidly lost BW, which stayed below that of the Base and Ctrl groups until euthanasia (Figure 2). Furthermore, the BTX injections resulted in substantial atrophy of the rectus femoris muscles compared to the Base and Ctrl groups (Table 1). Neither BTX nor pantoprazole

affected the length or height of the femora, humeri, and L5 vertebrae (Table 1).

Dual energy X-ray absorptiometry (DEXA)

Pantoprazole was not able to counteract the BTX-induced loss of femoral BMC and aBMD compared to the Base and Ctrl groups (Table 2). Unexpectedly, the mice injected with pantoprazole had a lower humeral aBMD than both the Base, Ctrl, and BTX groups (Table 2).

Micro computed tomography (μCT)

The BTX-injections resulted in a lower cortical bone area at the femoral mid-diaphysis compared to both the Base and Ctrl groups, which was caused by endosteal resorption as the marrow area of the BTX-injected groups was larger than that of the Ctrl group (Figure 3 and Table 3). The lower bone area
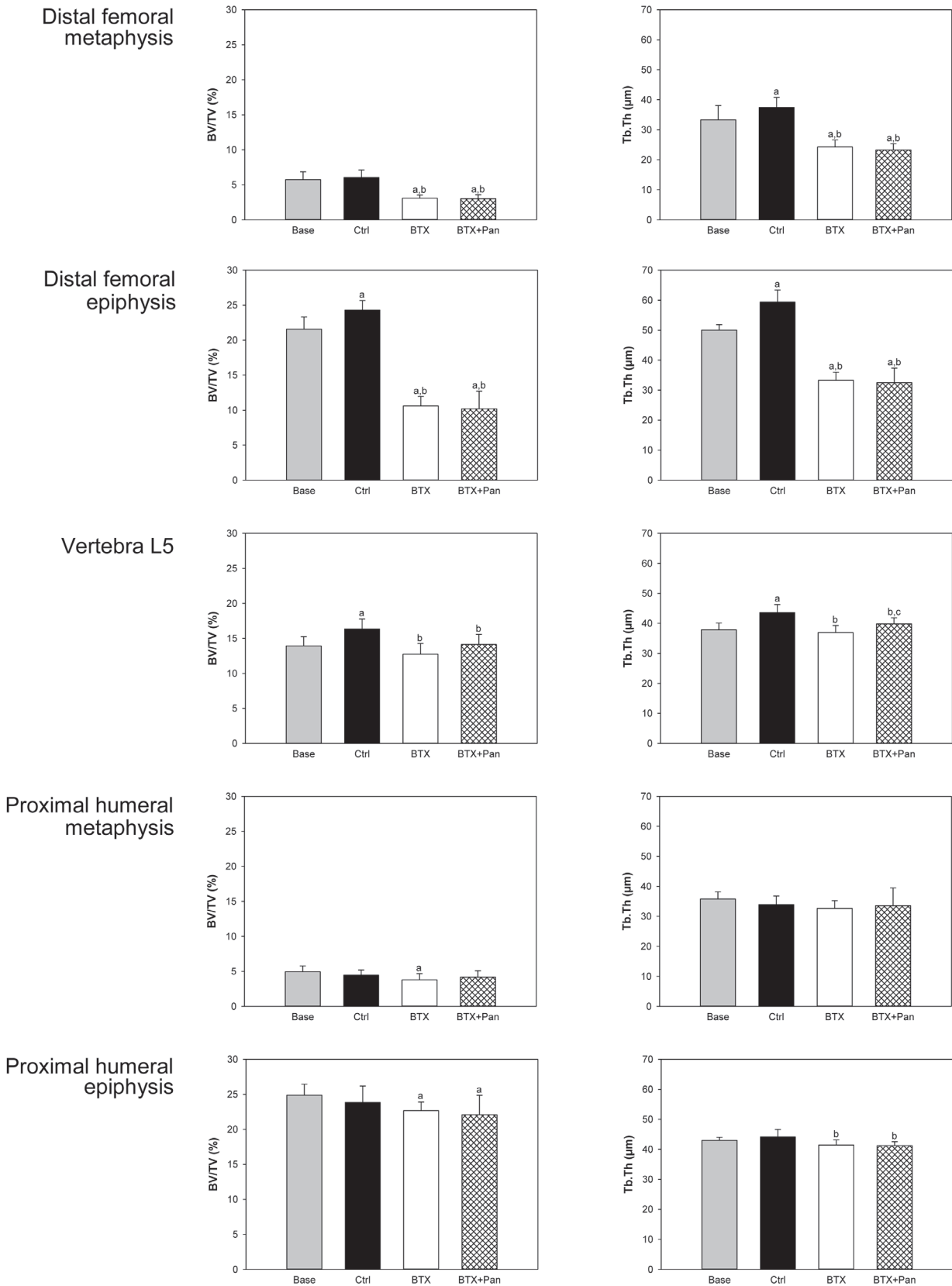
Figure 5. Trabecular bone volume fraction (BV/TV) and trabecular thickness (Tb.Th) of the analyzed VOI from the μCT scans that contains trabecular bone. [a] denotes a significant difference from Base, [b] donates a significant difference from Ctrl, and [c] denotes a significant difference from BTX. Mean $\pm$ SD.

Table 4. μCT of the distal femoral metaphysis and epiphysis, L5 vertebra, and proximal humeral metaphysis and epiphysis.

	BV/TV (%)	Tb.Th (μm)	Tb.N (1/mm)	Tb.Sp (μm)	CD (1/mm³)	SMI (-)	Bone material density (mg/cm³)
Distal femoral metaphysis							
Base	5.7 ± 1.1	33.3 ± 4.7	3.6 ± 0.2	276 ± 13	208 ± 38	2.3 ± 0.2	866 ± 15
Ctrl	6.0 ± 1.1	37.5 ± 3.3 [a]	3.4 ± 0.2 [a]	294 ± 14 [a]	157 ± 31 [a]	2.2 ± 0.2	882 ± 14 [a]
BTX	3.1 ± 0.5 [a,b]	24.2 ± 2.3 [a,b]	3.2 ± 0.1 [a,b]	313 ± 13 [a,b]	134 ± 24 [a]	2.3 ± 0.1	833 ± 11 [a,b]
BTX+Pan	3.0 ± 0.6 [a,b]	23.3 ± 2.1 [a,b]	3.2 ± 0.1 [a,b]	310 ± 15 [a,b]	145 ± 26 [a]	2.3 ± 0.1	825 ± 19 [a,b]
Distal femoral epiphysis							
Base	21.6 ± 1.7	50.0 ± 1.8	5.2 ± 0.4	212 ± 14	293 ± 48	0.3 ± 0.1	949 ± 8
Ctrl	24.3 ± 1.4 [a]	59.3 ± 4.0 [a]	5.0 ± 0.4	223 ± 17	212 ± 62 [a]	0.1 ± 0.1 [a]	968 ± 14 [a]
BTX	10.6 ± 1.4 [a,b]	33.3 ± 2.7 [a,b]	4.2 ± 0.3 [a,b]	245 ± 19 [a,b]	300 ± 50 [b]	0.9 ± 0.1 [a,b]	903 ± 14 [a,b]
BTX+Pan	10.2 ± 2.5 [a,b]	32.5 ± 4.8 [a,b]	4.0 ± 0.2 [a,b]	257 ± 17 [a,b]	321 ± 61 [b]	1.0 ± 0.2 [a,b]	893 ± 16 [a,b]
L5 Vertebra							
Base	13.9 ± 1.3	37.8 ± 2.3	3.8 ± 0.2	263 ± 17	267 ± 50	1.0 ± 0.1	924 ± 9
Ctrl	16.4 ± 1.4 [a]	43.6 ± 2.7 [a]	3.7 ± 0.2	265 ± 20	258 ± 50	0.9 ± 0.1 [a]	933 ± 8 [a]
BTX	12.7 ± 1.5 [b]	36.9 ± 2.4 [b]	3.5 ± 0.3	284 ± 25	253 ± 38	1.1 ± 0.2 [b]	928 ± 7
BTX+Pan	14.1 ± 1.4 [b]	39.8 ± 2.1 [b,c]	3.6 ± 0.3	279 ± 28	272 ± 51	1.1 ± 0.1 [b]	928 ± 5
Proximal humeral metaphysis							
Base	4.9 ± 0.8	35.8 ± 2.4	3.4 ± 0.2	292 ± 20	102 ± 26	2.4 ± 0.2	872 ± 9
Ctrl	4.5 ± 0.7	33.9 ± 2.9	3.2 ± 0.2 [a]	317 ± 19 [a]	83 ± 23	2.4 ± 0.1	872 ± 13
BTX	3.8 ± 0.9 [a]	32.6 ± 2.6	3.1 ± 0.2 [a]	323 ± 21 [a]	77 ± 20 [a]	2.5 ± 0.2	858 ± 17
BTX+Pan	4.2 ± 0.9	33.5 ± 5.9	3.1 ± 0.2 [a]	326 ± 20 [a]	84 ± 18	2.4 ± 0.2	862 ± 21
Proximal humeral epiphysis							
Base	24.9 ± 1.6	43.0 ± 1.0	6.3 ± 0.4	161 ± 11	438 ± 37	0.1 ± 0.1	919 ± 7
Ctrl	23.8 ± 2.3	44.2 ± 2.5	5.9 ± 0.5	173 ± 14 [a]	364 ± 47 [a]	0.0 ± 0.2	923 ± 14
BTX	22.7 ± 1.2 [a]	41.5 ± 1.7 [b]	5.8 ± 0.4 [a]	175 ± 11 [a]	410 ± 63	0.1 ± 0.1	915 ± 14
BTX+Pan	22.1 ± 2.8 [a]	41.3 ± 1.3 [b]	5.7 ± 0.5 [a]	179 ± 16 [a]	375 ± 61 [a]	0.1 ± 0.2	913 ± 11

Trabecular bone volume fraction (BV/TV). Trabecular thickness (Tb.Th). Trabecular number (Tb.N). Trabecular spacing (Tb.Sp). Connectivity density (CD). Structure model index (SMI). [a] denotes a significant difference from Base, [b] denotes a significant difference from Ctrl, and [c] denotes a significant difference from BTX. Mean±SD.

was followed by a lower polar moment of inertia in the BTX-injected groups compared to both the Base and Ctrl groups (Table 3). Moreover, the marrow area at the humeral mid-diaphysis expanded due to the BTX-injections when compared to both the Base and Ctrl groups (Figure 3 and Table 3). Pantoprazole did not prevent the loss of cortical bone.

At both the distal femoral metaphysis and epiphysis, the BTX-injections resulted in a bone loss indicated by lower BV/TV, Tb.Th, Tb.N, and bone material density and higher Tb.Sp compared to the Base and Ctrl groups (Figure 4, Figure 5, and Table 4). At the distal femoral epiphysis, the BTX-induced bone loss was accompanied by a higher SMI, indicating a shift towards more rod-like trabeculae, compared to the Base and Ctrl groups (Figure 4 and Table 4). At the L5 vertebral body, BTX resulted in a lower BV/TV and Tb.Th, and a slightly higher SMI, compared to the Ctrl group (Figure 4, Figure 5, and Table 4). At the proximal humeral metaphysis and epiphysis, BTX had a minor deleterious effect on the trabecular bone compared to the Base or Ctrl group (Figure 4, Figure 5, and Table 4). Only at the vertebra L5 did pantoprazole seem to

have a preventable effect on the loss of BV/TV and Tb.Th (Figure 5).

Mechanical testing

The BTX-injections resulted in a lower fracture strength and maximum stiffness at both the femoral mid-diaphysis and neck compared to the Base and Ctrl groups (Figure 6). At the L5 vertebra, the BTX group had lower fracture strength than both the Base and Ctrl groups, whereas the BTX+Pan group had a fracture strength that was lower than the Ctrl group only (Figure 6). At the humeral mid-diaphysis, the BTX-injected mice had lower fracture strength than the Ctrl group (Figure 6).
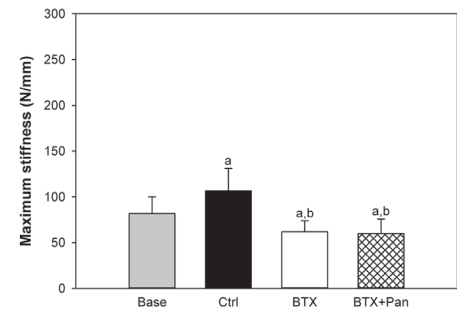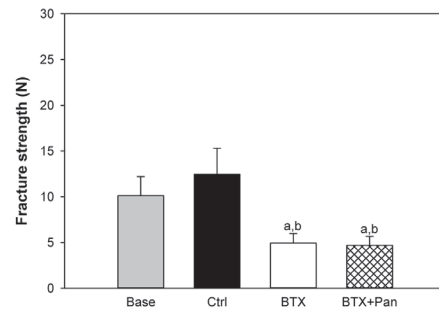
Dynamic bone histomorphometry

During day 13-17 of the study, BTX resulted in higher BFR/BS at both the distal femoral metaphysis and epiphysis compared to the Ctrl group (Table 5). At the distal femoral metaphysis, the higher BFR/BS was driven by a higher MAR,
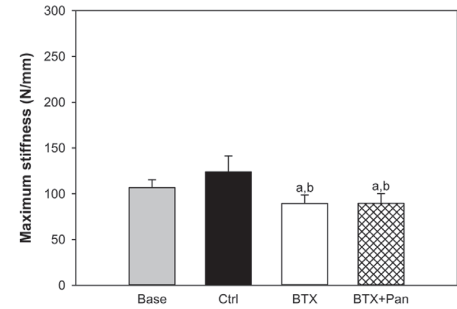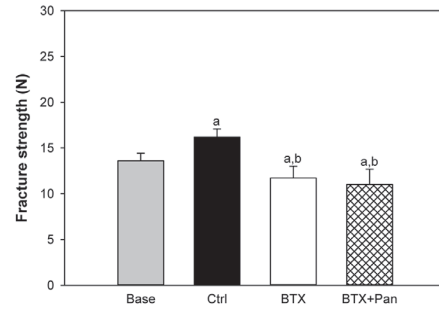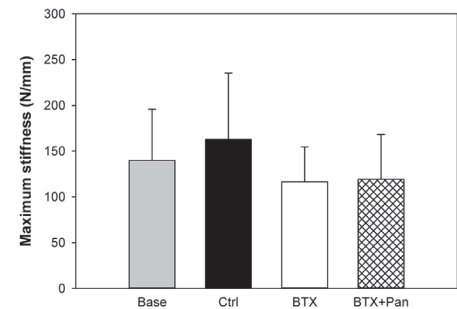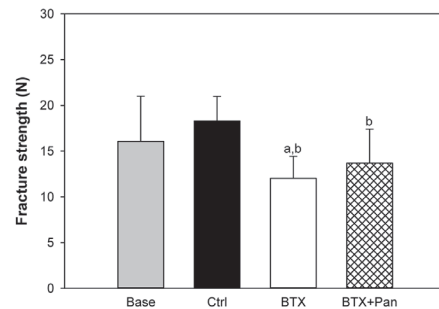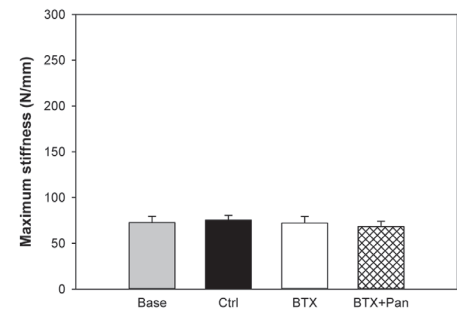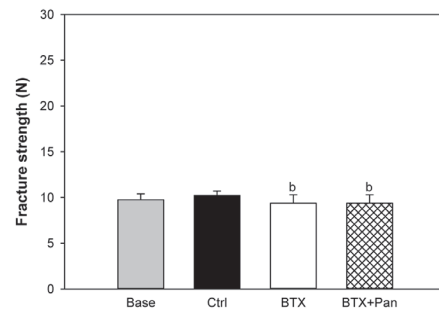
Figure 6. Fracture strength and maximum stiffness obtained by mechanical testing. [a] denotes a significant difference from Base and [b] donates a significant difference from Ctrl. Mean ± SD.

whereas at the distal femoral epiphysis the higher BFR/BS was a combination of both a higher MS/BS and MAR (Table 5). In general, during day 9-13 of the study, there was no or only minor indications of higher osteoblastic activity in the BTX-injected mice compared to the Ctrl group (Table 5). Treatment with pantoprazole did not have any effect on either MS/BS, MAR, or BFR/BS.

At euthanasia, neither BTX nor treatment with pantoprazole affected the Oc.S/BS (Figure 7).

Reverse transcription quantitative polymerase chain reaction (RT-qPCR)

At euthanasia, *Bglap*, which is the mRNA template that osteocalcin is translated from, was higher expressed in the distal tibia of the BTX-injected hind limb, indicating higher osteoblastic activity, compared to the Ctrl group (Figure 8). *Ctsk* and *Atp6vOd2*, which are translated to cathepsin K and the V-type proton ATPase subunit d2, respectively, were both

Table 5. Dynamic bone histomorphometry of the distal femoral metaphysis and epiphysis.

	Day 9-13			Day 13-17		
	MS/BS (%)	MAR (µm/d)	BFR/BS (µm³/µm²/d)	MS/BS (%)	MAR (µm/d)	BFR/BS (µm³/µm²/d)
Distal femoral metaphysis						
Base	-	-	-	-	-	-
Ctrl	37 ± 6	1.8 ± 0.2	0.7 ± 0.1	35 ± 7	2.0 ± 0.3	0.7 ± 0.2
BTX	28 ± 6 [b]	2.1 ± 0.7	0.6 ± 0.2	38 ± 8	2.5 ± 0.4 [b]	1.0 ± 0.3 [b]
BTX+Pan	29 ± 7 [b]	2.2 ± 0.5	0.6 ± 0.2	37 ± 3	2.6 ± 0.4 [b]	1.0 ± 0.2 [b]
Distal femoral epiphysis						
Base	-	-	-	-	-	-
Ctrl	56 ± 7	1.1 ± 0.1	0.6 ± 0.1	45 ± 12	1.2 ± 0.2	0.5 ± 0.2
BTX	51 ± 13	1.4 ± 0.2 [b]	0.7 ± 0.2	55 ± 7 [b]	1.6 ± 0.2 [b]	0.9 ± 0.1 [b]
BTX+Pan	51 ± 9	1.6 ± 0.2 [b]	0.8 ± 0.2 [b]	53 ± 7 [b]	1.7 ± 0.2 [b]	0.9 ± 0.1 [b]

Mineralizing surfaces (MS/BS). Mineral apposition rate (MAR). Bone formation rate (BFR/BS). [b] denotes a significant difference from Ctrl. Mean ± SD.
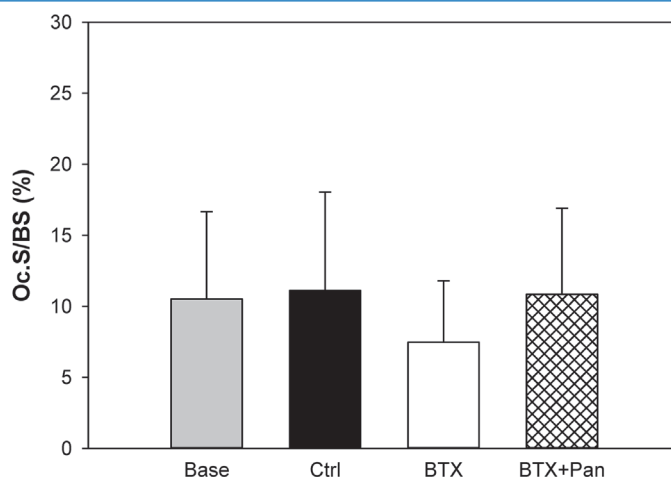
Figure 7. Osteoclast covered bone surfaces (Oc.S/BS) at the proximal tibial metaphysis. Mean ± SD.

higher expressed in the BTX-injected mice, indicating higher osteoclastic activity, compared to both the Base and Ctrl groups (Figure 8). The ratio of *Rankl/Opg*, which is an indicator of osteoclastic differentiation from the hematopoietic stem cell lineage, was higher in the BTX-injected groups than in the Ctrl group (Figure 8). *Nfatc1*, which is an indicator of osteoclastic differentiation, was not affected by BTX (Data not shown). Pantoprazole did not have any effect on osteoblastic or osteoclastic related gene expression.

Discussion

The present study did not demonstrate any bone specific effects of treatment with pantoprazole on either BTX induced disuse osteopenia or at the remaining intact skeleton in skeletally mature C57BL/6J female mice.

Pantoprazole does not prevent disuse osteopenia

The localized injections of BTX induced a profound and significant bone loss in the affected hind limb. In pre-clinical studies, pantoprazole has been shown to affect both osteoblasts and osteoclasts, which led to the hypothesis that pantoprazole might have a bone protective effect[9,25]. However, microstructural, mechanical, histological, and molecular analyses did not reveal any bone specific effects, although pantoprazole was given in a dose that is 100-200 times higher than therapeutic human doses.

PPIs irreversibly inhibit the gastric H^+/K^+-ATPase by covalently binding cysteine residues with disulfide bonds and thereby reducing the capacity for proton pumping[5]. Accordingly, PPIs might potentially inhibit the V-ATPase and thereby disrupt bone resorption. Furthermore, the different PPIs react with different cysteine residues, and this might
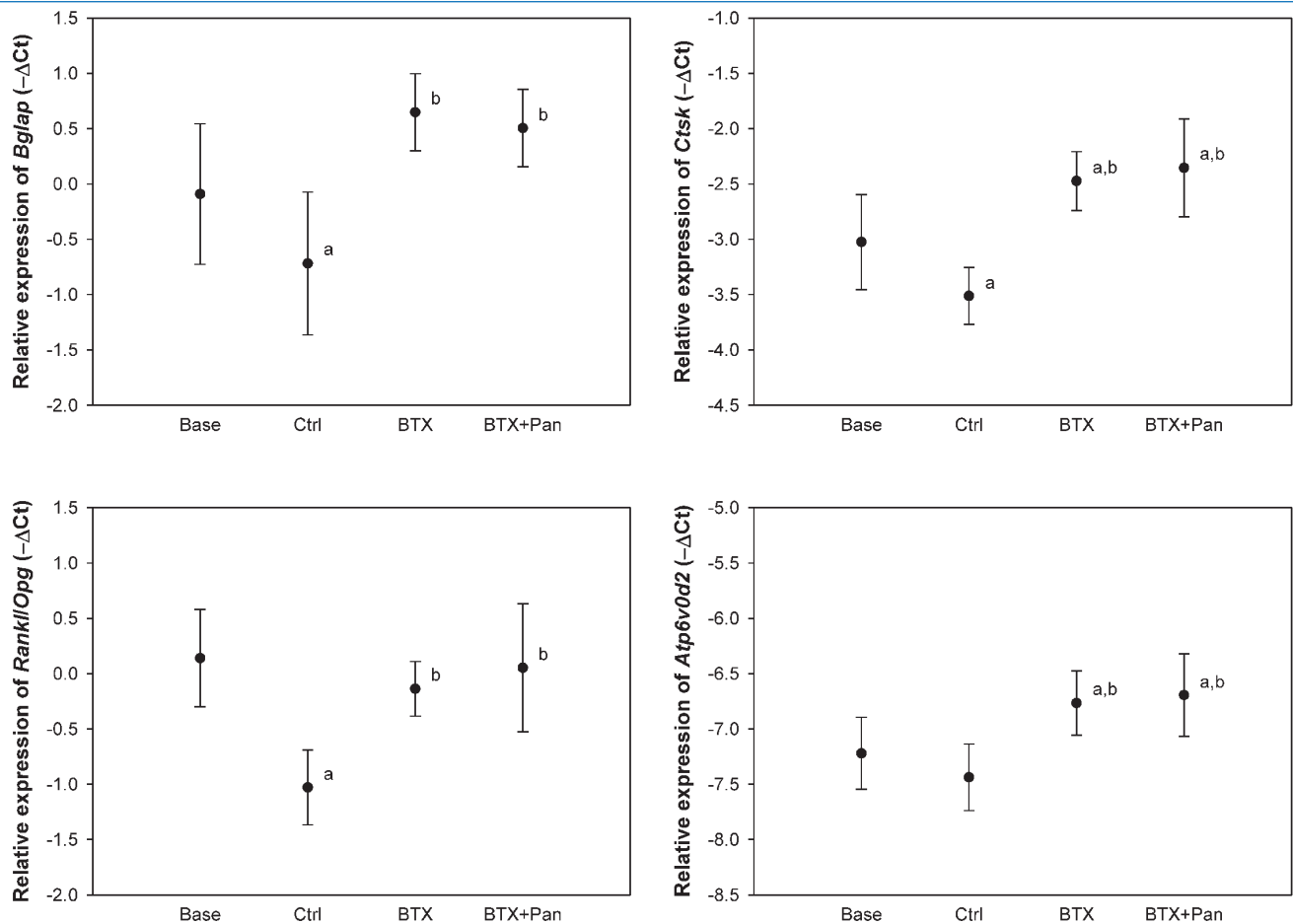
Figure 8. Relative gene expression obtained from the distal tibia. [a] denotes a significant difference from Base and [b] donates a significant difference from Ctrl. Mean ± SD.

be important for a possible osteoclast inhibiting effect[5]. However, *in vitro* experiments have shown an osteoclast inhibitory effect of both omeprazole[6-8,26], esomeprazole[8], lansoprazole[8], and pantoprazole[9].

In the present study, we chose to treat disuse osteopenia with pantoprazole based upon the study by Histing et al., in which daily pantoprazole injections impaired bone healing in a murine mid-femoral fracture model[14]. Most *in vivo* studies have been performed on rats, in which treatment with PPIs in young animals resulted in lower BMC[27-29], whereas PPIs seemed to have either no or a bone protective effect in intact and gastrectomized older animals[11,30]. Moreover, PPIs have been associated with reduced expression of osteoclast specific mRNA, osteoclast numbers, and resorption of calcium cements[13,15,31]. However, the present study was not able to detect any of these osteoclast specific effects of PPI treatment on microstructural properties, gene expression, or Oc.S/BS in either the intact or the disuse osteopenic mouse skeleton.

Although the hypothesis of the present study was that the PPI pantoprazole would have an osteoprotective effect,

current literature suggests an increased incidence of osteoporotic fractures following both short and long-term PPI treatment in a clinical setting[32,33]. The biological explanation has been proposed to be a decrease in calcium and magnesium uptake due to higher gastric pH induced by PPI treatment[34,35], increase in the incidence of falls leading to fragility fractures[36], and a direct effect on bone cells[37]. However, the studies are conflicting and a persuasive biological explanation remains to be found[32,33,38,39]. Furthermore, most of the clinical studies are observational and confounding due to e.g. polypharmacy and multi-morbidity might explain the increased fracture risk in PPI users rather than the drug itself.

The systemic skeletal effects of localized botulinum toxin injections are widespread

In the present study, we investigated both the disuse osteopenic hind limb, and the L5 vertebral body and humerus located distant from the BTX-injected limb, in order to elucidate any bone specific effects of the pantoprazole treatment. Although pantoprazole did not have any bone

specific effects, we found that the BTX induced disuse affected the supposedly intact skeleton at bone sites distant from the paralyzed muscles. Both the L5 vertebral body and humerus had deteriorated microstructural and mechanical properties because of the BTX injections.

Systemic effects of the localized intramuscular injections of BTX have been reported several times and seems to be a consistent finding[19,21,22,40-44]. The effects range from small differences in BW between BTX injected and control mice to substantial muscle and bone wasting of the non-injected contralateral hind limb compared to control mice. The present study is the first to report widespread skeletal systemic effects in the spine and humerus. However, the bone loss in the immobilized hind limb by far outweighs any systemic effects.

Tail suspension (TS) and sciatic neurectomy (SN) are also widely used to study disuse osteopenia in mice. TS remove the ground reaction force on the hind limbs, but not the muscle forces, by elevating the rearmost part of the mouse body. SN paralyzes not only the muscles innervated by the sciatic nerve, but also disrupts the autonomic and sensory nervous system associated. A systemic skeletal effect of unloading is also seen with TS and SN induced disuse osteopenia. TS induces lower bone mass and bone strength of the vertebra and humerus compared to control mice[45,46], whereas only the vertebral bone loss has been investigated in SN[47]. It is not surprising that hind limb immobilization causes lower bone mass and bone strength in the lumbar vertebrae with BTX, TS, and SN induced disuse osteopenia, as loads and muscle forces exerted on the spine are altered. However, it is surprising that the humerus, which must bear more loads, especially with TS, is negatively affected by disuse. A possible explanation for this might be systemically uptake of botulinum toxin, reduced food intake, decreased ambulation, increased levels of glucocorticoids and other catabolic stress hormones, and "spill-over" of bone acting molecules from the immobilized hind limb. Recently, the muscle-bone interaction has attracted much attention and molecules secreted by skeletal muscles, i.e. myokines, are recognized as important factors in regulating bone homeostasis and turnover[48]. In the present study, BTX induced a massive muscle loss and myokines secreted during atrophy might influence bone health at distant skeletal sites and explain the widespread systemic effect.

Limitations and future perspectives

The present study did not find any bone specific effects of pantoprazole, which might be related to the short study duration or that pantoprazole does not have a direct inhibiting effect on the osteoclastic V-ATPase. The duration of the present study was chosen based on earlier investigations of BTX-induced osteopenia, which showed that the BTX-induced bone loss levels out after three weeks[17,40]. Long-term treatment in intact, fully-grown mice might elucidate bone specific effects and help explain the clinically observed PPI treatment related increased fracture risk. Furthermore, the substantial and rapid bone loss induced by BTX might

overshadow any osteoclast inhibiting effects of pantoprazole. However, as no substantial effect was observed at the skeletal sites distant from the immobilized hind limb, it seems unlikely that pantoprazole directly influences bone cell function in mice. We interpret the minor, but significant, bone-protecting effect of pantoprazole seen on the trabecular thickness of the L5 vertebral body as a statistical type-1 error.

The widespread systemic effects on the non-immobilized skeleton are interesting and the biological mechanism remains to be found. The explanation might just be reduced food intake and reduced BW, but hormonal factors, e.g. myokines, cannot be ruled out and insights might provide new drug targets.

Conclusion

The PPI pantoprazole was unable to prevent the development of BTX induced disuse osteopenia in skeletally mature female C57BL/6J mice.

References

1. Sobacchi C, Schulz A, Coxon FP, Villa A, Helfrich MH. Osteopetrosis: genetics, treatment and new insights into osteoclast function. Nat Rev Endocrinol 2013; 9:522-536.
2. Villa A, Guerrini MM, Cassani B, Pangrazio A, Sobacchi C. Infantile malignant, autosomal recessive osteopetrosis: The rich and the poor. Calcif Tissue Int 2009;84:1-12.
3. Qin A, Cheng TS, Pavlos NJ, Lin Z, Dai KR, Zheng MH. V-ATPases in osteoclasts: Structure, function and potential inhibitors of bone resorption. Int J Biochem Cell Biol 2012;44:1422-1435.
4. Cotter K, Stransky L, McGuire C, Forgac M. Recent insights into the structure, regulation, and function of the V-ATPases. Trends Biochem Sci 2015;40:611-622.
5. Kopic S, Geibel JP. Gastric acid, calcium absorption, and their impact on bone health. Physiol Rev 2013; 93:189-268.
6. Tuukkanen J, Vaananen HK. Omeprazole, a specific inhibitor of H⁺-K⁺-ATPase, inhibits bone resorption *in vitro*. Calcif Tissue Int 1986;38:123-125.
7. Zaidi M. Modularity of osteoclast behaviour and 'mode-

specific' inhibition of osteoclast function. Biosci Rep 1990;10:547-556.

8. Costa-Rodrigues J, Reis S, Teixeira S, Lopes S, Fernandes MH. Dose-dependent inhibitory effects of proton pump inhibitors on human osteoclastic and osteoblastic cell activity. FEBS J 2013;280:5052-5064.

9. Prause M, Seeliger C, Unger M, Rosado Balmayor E, van Griensven M, Haug AT. Pantoprazole decreases cell viability and function of human osteoclasts *in vitro*. Mediators Inflamm 2015;2015:413097.

10. Håkanson R, Persson P, Axelson J, Johnell O, Sundler F. Evidence that gastrin enhances 45Ca uptake into bone through release of a gastric hormone. Regul Pept 1990;28:107-118.

11. Persson P, Gagnemo-Persson R, Chen D, Axelson J, Nylander AG, Johnell O, Häkanson R. Gastrectomy causes bone loss in the rat: Is lack of gastric acid responsible? Scand J Gastroenterol 1993;28:301-306.

12. Pytlik M, Cegieła U, Folwarczna J, Nowińska B. Proton pump (H^+/K^+-ATPase) inhibitors weaken the protective effect of alendronate on bone mechanical properties in estrogen-deficient rats. Pharmacol Reports 2012; 64:625-634.

13. Joo MK, Park JJ, Lee BJ, Kim JH, Yeon JE, Kim JS, Byun KS, Bak YT. The effect of a proton pump inhibitor on bone metabolism in ovariectomized rats. Mol Med Rep 2013;7:1267-1272.

14. Histing T, Stenger D, Scheuer C, Metzger W, Garcia P, Holstein JH, Klein M, Pohlemann T, Menger MD.Pantoprazole, a proton pump inhibitor, delays fracture healing in mice. Calcif Tissue Int 2012;90:507-14.

15. Sheraly AR, Lickorish D, Sarraf F, Davies JE. Use of gastrointestinal proton pump inhibitors to regulate osteoclast-mediated resorption of calcium phosphate cements *in vivo*. Curr Drug Deliv 2009;6:192-198.

16. Krølner B, Toft B. Vertebral bone loss: An unheeded side effect of therapeutic bed rest. Clinical science (London, England: 1979) 1983;64:537-540.

17. Vegger JB, Brüel A, Dahlgaard AF, Thomsen JS. Alterations in gene expression precede sarcopenia and osteopenia in botulinum toxin immobilized mice. J Musculoskelet Neuronal Interact 2016;16:355-368.

18. Chappard D, Chennebault A, Moreau M, Legrand E, Audran M, Basle MF. Texture analysis of X-ray radiographs is a more reliable descriptor of bone loss than mineral content in a rat model of localized disuse induced by the clostridium botulinum toxin. Bone 2001;28:72-79.

19. Warner SE, Sanford DA, Becker BA, Bain SD, Srinivasan S, Gross TS. Botox induced muscle paralysis rapidly degrades bone. Bone 2006;38:257-264.

20. Thomsen JS, Christensen LL, Vegger JB, Nyengaard JR, Brüel A. Loss of bone strength is dependent on skeletal site in disuse osteoporosis in rats. Calcif Tissue Int 2012;90:294-306.

21. Lodberg A, Vegger JB, Jensen MV, Larsen CM, Thomsen JS, Brüel A. Immobilization induced bone loss is strain specific in mice. Bone Reports 2015;2:59-67.

22. Vegger JB, Brüel A, Brent MB, Thomsen JS. Disuse osteopenia induced by botulinum toxin is similar in skeletally mature young and aged female C57BL/6J mice. J Bone Miner Metab 2017:[Epub ahead of print].

23. Bouxsein ML, Boyd SK, Christiansen BA, Guldberg RE, Jepsen KJ, Müller RJ. Guidelines for assessment of bone microstructure in rodents using micro-computed tomography. J Bone Miner Res 2010;25:1468-1486.

24. Vegger JB, Nielsen ES, Brüel A, Thomsen JS. Additive effect of PTH (1-34) and zoledronate in the prevention of disuse osteopenia in rats. Bone 2014;66:287-295.

25. Prause M, Seeliger C, Unger M, Van Griensven M, Haug AT. Pantoprazole increases cell viability and function of primary human osteoblasts *in vitro*. Injury 2014; 45:1156-1164.

26. Mattsson JP, Väänänen K, Wallmark B, Lorentzon P. Omeprazole and bafilomycin, two proton pump inhibitors: Differentiation of their effects on gastric, kidney and bone H(+)-translocating ATPases. Biochim Biophys Acta 1991;1065:261-268.

27. Cui GL, Syversen U, Zhao CM, Chen D, Waldum HL. Long-term omeprazole treatment suppresses body weight gain and bone mineralization in young male rats. Scand J Gastroenterol 2001;36:1011-1015.

28. Takasugi S, Ashida K, Maruyama S, Komaba Y, Kaneko T, Yamaji T. A dairy product fermented by lactobacilli cancels the adverse effects of hypochlorhydria induced by a proton pump inhibitor on bone metabolism in growing rats. Br J Nutr 2011;106:1487-1494.

29. Dobrowolski P, Tomaszewska E, Radzki RP, Bienko M, Wydrych J, Zdybel A, Pierzynowski SG. Can 2-oxoglutarate prevent changes in bone evoked by omeprazole? Nutrition 2013;29:556-561.

30. Yamasaki Y, Fujimura T, Oyama K, Higashi Y, Hirose A, Tsukada T, Okamoto K, Kinoshita J, Nakamura K, Miyashita T, Tajima H, Takamura H, Ninomiya I, Fushida S, Ohta T. Effects of rabeprazole on bone metabolic disorders in a gastrectomized rat model. Biomed Reports 2016;5:118-124.

31. Al Subaie A, Emami E, Tamimi I, Laurenti M, Eimar H, Abdallah MN, Tamimi F. Systemic administration of omeprazole interferes with bone healing and implant osseointegration: An *in vivo* study on rat tibiae. J Clin Periodontol 2016;43:193-203.

32. Zhou B, Huang Y, Li H, Sun W, Liu J. Proton-pump inhibitors and risk of fractures: An update meta-analysis. Osteoporos Int 2016;27:339-347.

33. Andersen BN, Johansen PB, Abrahamsen B. Proton pump inhibitors and osteoporosis. Curr Opin Rheumatol 2016;28:420-425.

34. O'Connell MB, Madden DM, Murray AM, Heaney RP, Kerzner LJ. Effects of proton pump inhibitors on calcium carbonate absorption in women: A randomized crossover trial. Am J Med 2005;118:778-781.

35. Cheungpasitporn W, Thongprayoon C, Kittanamongkolchai W, Srivali N, Edmonds PJ, Ungprasert P, O'Corragain

OA, Korpaisarn S, Erickson SB. Proton pump inhibitors linked to hypomagnesemia: A systematic review and meta-analysis of observational studies. Ren Fail 2015; 37:1237-1241.

36. Lewis JR, Barre D, Zhu K, Ivey KL, Lim EM, Hughes J, Prince RL. Long-term proton pump inhibitor therapy and falls and fractures in elderly women: A prospective cohort study. J Bone Miner Res 2014;29:2489-2497.

37. Jo Y, Park E, Ahn SB, Jo YK, Son B, Kim SH, Park YS, Kim HJ. A proton pump inhibitor's effect on bone metabolism mediated by osteoclast action in old age: A prospective randomized study. Gut Liver 2014;9:607-614.

38. Hansen KE, Jones AN, Lindstrom MJ, Davis LA, Ziegler TE, Penniston KL, Alvig AL, Shafer MM. Do proton pump inhibitors decrease calcium absorption? J Bone Miner Res 2010;25:2510-2519.

39. Wright MJ, Sullivan RR, Gaffney-Stormberg E, Caseria DM, O'Brien KO, Proctor DD, Simpson CA, Kerstetter JE, Insogna KL. Inhibiting gastric acid production does not affect intestinal calcium absorption in young, healthy individuals: A randomized, crossover, controlled clinical trial. J Bone Miner Res 2010;25:2205-2211.

40. Grimston SK, Silva MJ, Civitelli R. Bone loss after temporarily induced muscle paralysis by botox is not fully recovered after 12 weeks. Ann N Y Acad Sci 2007;1116:444-460.

41. Manske SL, Boyd SK, Zernicke RF. Muscle changes can account for bone loss after botulinum toxin injection. Calcif Tissue Int 2010;87:541-549.

42. Poliachik SL, Bain SD, Threet D, Huber P, Gross TS. Transient muscle paralysis disrupts bone homeostasis by rapid degradation of bone morphology. Bone 2010; 46:18-23.

43. Aliprantis AO, Stolina M, Kostenuik PJ, Poliachik SL, Warner SE, Bain SD, Gross TS. Transient muscle paralysis degrades bone via rapid osteoclastogenesis. FASEB J 2012;26:1110-1118.

44. Ellman R, Grasso DJ, van Vliet M, Brooks DJ, Spatz JM, Conlon C, Bouxsein ML. Combined effects of botulinum toxin injection and hind limb unloading on bone and muscle. Calcif Tissue Int 2014;94:327-337.

45. Simske SJ, Greenberg AR, Luttges MW. Effects of suspension-induced osteopenia on the mechanical behaviour of mouse long bones. J Mater Sci Mater Med 1991;2:43-50.

46. Alwood JS, Yumoto K, Mojarrab R, Limoli CL, Almeida EA, Searby ND, Globus RK. Heavy ion irradiation and unloading effects on mouse lumbar vertebral microarchitecture, mechanical properties and tissue stresses. Bone 2010;47:248-255.

47. Ko CY, Jung YJ, Seo DH, Schreiber J, Lim D, Kim HS. Trabecular bone loss in lumbar vertebrae and tibiae following sciatic nerve injury: Correlation between baseline bone quantity (BV/TV) and the magnitude and rate of bone loss. Int J Precis Eng Manuf 2012; 13:1705-1708.

48. Guo B, Zhang ZK, Liang C, Li J, Liu J, Lu A, Zhang BT, Zhang G. Molecular communication from skeletal muscle to bone: A review for muscle-derived myokines regulating bone metabolism. Calcif Tissue Int 2017;100:184-192.